Proceedings of the Estonian Academy of Sciences,
2010, **59**, 2, 118–125
doi: 10.3176/proc.2010.2.09
Available online at www.eap.ee/proceedings

MECHANICS

On the propagation of solitary waves in Mindlin-type microstructured solids

Kert Tamm[a,b] and Andrus Salupere[a,b*]

[a] Centre for Nonlinear Studies, Institute of Cybernetics at Tallinn University of Technology, Akadeemia tee 21, 12618 Tallinn, Estonia
[b] Department of Mechanics, Tallinn University of Technology, Ehitajate tee 5, 19086 Tallinn, Estonia; kert@cens.ioc.ee

Received 10 December 2009, accepted 3 February 2010

Abstract. The Mindlin–Engelbrecht–Pastrone model is applied to simulating 1D wave propagation in microstructured solids. The model takes into account the nonlinearity in micro- and macroscale. Numerical solutions are found for the full system of equations (FSE) and the hierarchical equation (HE). The latter is derived from the FSE by making use of the slaving principle. Analysis of results demonstrates good agreement between the solutions of the FSE and HE in the considered domain of parameters. For numerical integration the pseudospectral method is used.

Key words: nonlinearity, microstructured solids, solitons, dispersion, pseudospectral methods.

1. INTRODUCTION

Microstructured materials are characterized by the existence of intrinsic space-scales in matter, like the lattice period, the size of a grain or a crystallite, or the distance between the microcracks, etc., which introduce the scale-dependence into the governing equations (see, e.g., [3,5,15,22,23] and references therein). The scale-dependence involves dispersive as well as nonlinear effects. If these two effects are balanced, solitons and solitary waves can exist in such media.

For numerical simulation of wave propagation in nonlinear dispersive media with the microstructure a model derived by Engelbrecht and Pastrone [2,11,12] is employed in the present paper. The model is based on Mindlin's and Eringen's earlier works [4,17]. In this approach the microelement is taken as a deformable cell and balance laws are formulated separately for macro- and microscale. At first the Lagrangian

$$L = K - W, \quad K = \frac{1}{2}\rho u_t^2 + \frac{1}{2} I \varphi_t^2, \quad W = W(u_x, \varphi, \varphi_x), \tag{1}$$

is introduced. Here K is the kinetic energy, W is the free energy, I is the microinertia, φ is the microdeformation, u is the macrodisplacement, ρ is the macroscale density, and partial derivatives are denoted by subscripts. In order to take into account the nonlinearity in micro- and macroscale, the free energy W can be written as follows:

$$W = \frac{A}{2}u_x^2 + \frac{B}{2}\varphi^2 + \frac{C}{2}\varphi_x^2 + D\varphi u_x + \frac{N}{6}u_x^3 + \frac{M}{6}\varphi_x^3. \tag{2}$$

* Corresponding author, salupere@ioc.ee

Here A,B,C,D are material parameters responsible for the linear part of the model and N,M are responsible for the nonlinearity in macro- and microscale, respectively [11,12]. Making use of the free energy function (2) and Euler–Lagrange equations, we obtain the equations of motion

$$\rho u_{tt} = D\varphi_x + Au_{xx} + Nu_x u_{xx}, \quad I\varphi_{tt} = C\varphi_{xx} + M\varphi_x\varphi_{xx} - B\varphi - Du_x. \tag{3}$$

For further analysis dimensionless variables $X = x/L_o$, $T = (\sqrt{A}t)/(\sqrt{\rho}L_o)$, $U = u/U_o$, $\delta = l_o^2/L_o^2$, $\varepsilon = U_o/L_o$ are introduced [11,12]. Here U_o and L_o are the amplitude and the wavelength of the initial excitation, and l_o is the characteristic scale of the microstructure. All together we have eleven different parameters – eight of them are material (six free energy parameters, macroscale density, and microinertia) and three are geometrical (the amplitude and wavelength of the initial excitation and the scale of the microstructure). The change of variables results in the dimensionless equations of motion

$$U_{TT} = \frac{DL_o}{AU_o}\varphi_X + \frac{NU_o}{AL_o}U_X U_{XX} + U_{XX}, \quad \varphi_{TT} = \frac{C\rho}{AI}\varphi_{XX} - \frac{B\rho L_o^2}{AI}\varphi - \frac{D\rho U_o L_o}{AI}U_X + \frac{M\rho}{AIL_o}\varphi_X\varphi_{XX}. \tag{4}$$

Equations (4) are referred to as the full system of equations (FSE for short) below. By applying the slaving principle [3,21], a single equation can be derived in terms of the macrodisplacement U from the FSE:

$$U_{TT} - bU_{XX} - \frac{\mu}{2}\left(U_X^2\right)_X = \delta\left(\beta U_{TT} - \gamma U_{XX} + \frac{\lambda\sqrt{\delta}}{2}U_{XX}^2\right)_{XX}. \tag{5}$$

Equation (5) is written in the form that makes its hierarchical nature (in Whitham's sense) clearly visible. In terms of material and geometrical parameters, constants in (5) are: $b = 1-(D^2/AB)$, $\mu = (NU_o)/(AL_o)$; $\beta = (ID^2)/(\rho l_o^2 B^2)$, $\gamma = (CD^2)/(AB^2 l_o^2)$, $\lambda = (D^3 M U_o)/(AB^3 l_o^3 L_o)$. Equation (5) can be considered as an approximation of FSE (4) and is referred to as the hierarchical equation (HE) below. On the other hand, HE (5) is of Boussinesq type [1].

In papers [26–28] we studied the interaction and solitonic character of emerging solitary waves in case of the HE. The main aim of this paper is to compare the propagation of sech^2-type solitary waves in the Mindlin-type microstructured solid for the HE and FSE in the range of parameters where both the macro- and microstructure are to be taken into account. The existence of the solution of the inverse solitary wave problem for the HE is proved in [11]. Therefore it is important to estimate the accuracy of the approximation (the HE) in the domain of parameters where dispersion curves for the HE and FSE differ less than 5%.

The paper is organized as follows. In Section 2 the problem is stated and the numerical technique is described. Results are presented in Section 3 and conclusions are drawn in Section 4.

2. STATEMENT OF THE PROBLEM AND NUMERICAL TECHNIQUE

In order to simulate numerically the propagation of solitary waves in Mindlin-type microstructured solids, HE (5) and FSE (4) are numerically integrated under sech^2-type localized initial conditions and periodic boundary conditions

$$U(X,0) = U_o \operatorname{sech}^2 \kappa X, \quad U(X,T) = U(X+2m\pi,T), \quad m = 1,2,3,\ldots. \tag{6}$$

For the amplitude and width of the initial pulse we use the values $U_o = 1$ and $\kappa = \pi/2$. For numerical integration the pseudospectral method based on the discrete Fourier transform (DFT) is used. Periodic boundary conditions have period of 12π, i.e., $m = 6$ in (6). Initial phase speed is taken to be zero, which can be interpreted as starting from the peak of the interaction of two waves propagating in opposite directions. For the FSE two more initial conditions are needed for the microdeformation. We assume that at $T = 0$ the microdeformation and the corresponding velocity are zero, i.e. $\varphi(X,0) = 0$ and $\varphi_T(X,0) = 0$.

The goals of the present paper are: (i) to solve HE (5) and FSE (4) under localized initial conditions for the weak normal dispersion case; (ii) to compare solutions of the HE and FSE for the linear and the nonlinear case; (iii) to compare solutions of the HE and FSE along a weak normal dispersion line (see Section 3 for details).

The DFT-based pseudospectral method (PSM) [6,14,24,25] is applied in numerical integration in the present paper. In a nutshell, the idea of the PSM is to approximate space derivatives making use of the DFT and then to use standard ODE solvers for integration with respect to time. However, the regular PSM algorithm is derived for $u_t = \Phi(u, u_x, u_{2x}, \ldots, u_{mx})$ type equations, but we have also a mixed partial derivative term $\delta\beta U_{TTXX}$ in HE (5) and therefore the standard PSM has to be modified [9,10,24,26,28]. Therefore we rewrite HE (5) so that all partial derivatives with respect to time are in the LHS of the HE, and introduce a new variable $\Phi = U - \delta\beta U_{XX}$. After that, making use of properties of the DFT, we can express the variable U and its spatial derivatives in terms of the new variable Φ:

$$U = \mathrm{F}^{-1}\left[\frac{\mathrm{F}(\Phi)}{1+\delta\beta k^2}\right], \quad \frac{\partial^m U}{\partial x^m} = \mathrm{F}^{-1}\left[\frac{(ik)^m \mathrm{F}(\Phi)}{1+\delta\beta k^2}\right]. \tag{7}$$

Here F denotes the DFT, F^{-1} the inverse DFT, $k = \pm 1, \pm 2, \ldots \pm (n/2-1), -n/2$, and n is the number of space-grid points. Finally, equation (5) can be rewritten in terms of the variable Φ:

$$\Phi_{TT} = bU_{XX} + \frac{\mu}{2}\left(U_X^2\right)_X - \delta\left(\gamma U_{XX} - \frac{\lambda\sqrt{\delta}}{2}U_{XX}^2\right)_{XX}. \tag{8}$$

In equation (8) all partial derivatives of U with respect to X are calculated in terms of Φ by making use of the expression (7). Therefore one can apply the PSM for numerical integration of equation (8). Full system of equations (4) is reduced to the system of first-order differential equations which are solved by the standard PSM without any further modifications.

In the present paper calculations are carried out with the Python package SciPy [13], using the FFTW library [7] for the DFT and the F2PY [20] generated Python interface to the ODEPACK Fortran code [8] for the ODE solver.

3. RESULTS

The dispersion type for the HE can be determined by the sign of the quantity $\Gamma = 1 - \gamma_1^2 - \gamma_A^2$, where $\gamma_A^2 = (D^2)/(AB)$, $\gamma_1^2 = (\rho C)/(AI)$; see [3] for details. One can interpret γ_1 as the dimensionless speed of short waves and $\sqrt{1-\gamma_A^2}$ as the dimensionless speed of long waves. If Γ is positive, we have the normal dispersion case, if Γ is negative, we have the anomalous dispersion case, and if Γ is equal to zero, we have the dispersionless case.

According to the dispersion analysis carried out in [19], acoustic branches of the HE and FSE are close to each other in the area between solid curves in Fig. 1, which corresponds to 5% difference between acoustic branches for the dimensionless wavenumber $\xi = 1.5$ ($\xi = k\sqrt{(AI)/(B\rho)}$, where k is the wavenumber). The FSE also has a second, so-called 'optical' branch. The dotted line corresponds to parameter combinations that result in the dispersionless case for acoustic branches. We have solved the stated problem for values of material and geometrical parameters that result in $\gamma_A^2 - \gamma_1^2$ plane points along the line $\Gamma = 0.05$ (Fig. 1). Here we discuss three cases in detail: points P1, P9, and P18 in Fig. 1. For the nonlinear case we define an additional parameter $\gamma_N = \lambda/\mu = (D^3 M)/(B^3 N l_o^3)$, describing the relation between nonlinearity in macro- and microscale. According to equation (5), λ is responsible for the microscale nonlinearity and μ for the macroscale nonlinearity. In the nonlinear case material parameters M and N are chosen so that $\gamma_N = 0.5$.

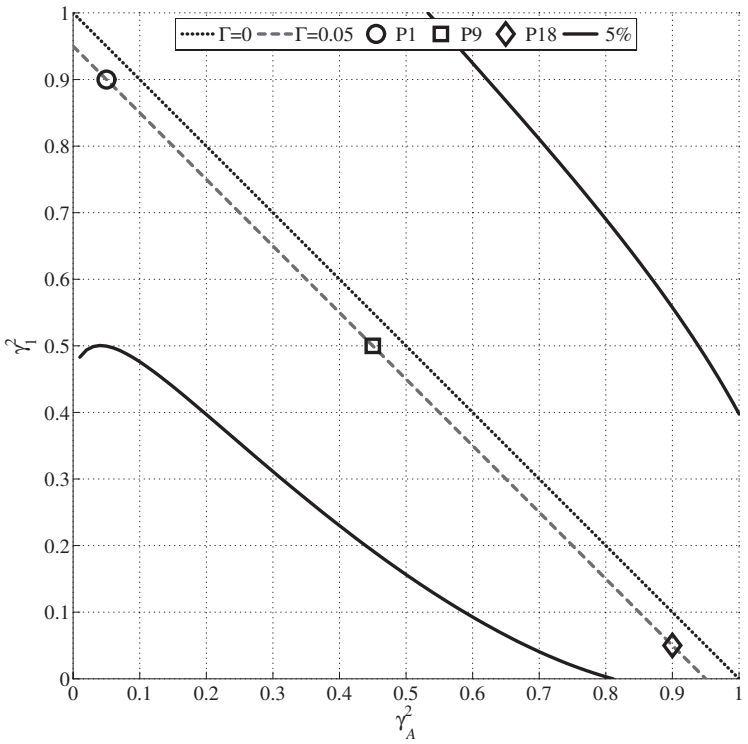

Fig. 1. Domain in the γ_A^2–γ_1^2 plane where the difference between acoustic branches of dispersion curves for the HE and FSE is less than 5%.

Nondimensional material parameters $\widehat{A}=12$, $\widehat{C}=9$, $\widehat{D}=5$, $\widehat{N}=1$, $\widehat{\rho}=10$, and geometrical parameters $\widehat{l_o}=1$, $\widehat{L_o}=50$, $\widehat{U_o}=1$ for all cases. The parameters $\widehat{I}$, $\widehat{B}$, $\widehat{M}$ vary, giving the following values for γ_A^2 and γ_1^2:

$$\begin{aligned}
&\text{P1}: \gamma_A^2=0.05; \quad \gamma_1^2=0.90; \quad \widehat{B}=125/3; \quad \widehat{I}=25/3; \quad \widehat{M}=15625/54;\\
&\text{P9}: \gamma_A^2=0.45; \quad \gamma_1^2=0.50; \quad \widehat{B}=125/27; \quad \widehat{I}=15; \quad \widehat{M}=15625/39966;\\
&\text{P18}: \gamma_A^2=0.90; \quad \gamma_1^2=0.05; \quad \widehat{B}=125/54; \quad \widehat{I}=150; \quad \widehat{M}=15625/314928.
\end{aligned} \tag{9}$$

The parameter $\gamma_N=0.5$ in the nonlinear case and has no value in the linear case (in the linear case N and M are zero). The integration interval is from zero to $T_f=100$. In all considered cases two solitary waves that propagate in opposite directions emerge from the initial pulse (6). For point P1 five interactions between the emerged solitary waves take place in the time interval $0<T\leq 100$. For points P9 and P18 the number of interactions in the time interval $0<T\leq 100$ is three and one, respectively.

3.1. Numerical results

Dispersion analysis carried out in [19] shows good agreement between acoustic branches of the HE and FSE at the chosen datapoints. However, it does not take into account the optical branch of the FSE and nonlinear effects. At P1 we can see that agreement between solutions of the HE and FSE is almost perfect even after five interactions of the two emerged solitary waves (Fig. 2). The left pulse in Fig. 2 is propagating to the right and the right pulse to the left. Analysis of the results demonstrates that in the linear case (lighter curves) the right and the left propagating waves are practically identical. However, in nonlinear cases (darker curves) the solitary waves propagating to the right are sharper, narrower, and slightly lower than the right propagating solitary waves in linear cases. Vice versa, the pulses propagating to the left are wider in nonlinear cases. The waveprofiles that correspond to the HE and the waveprofiles that correspond to the FSE practically coincide

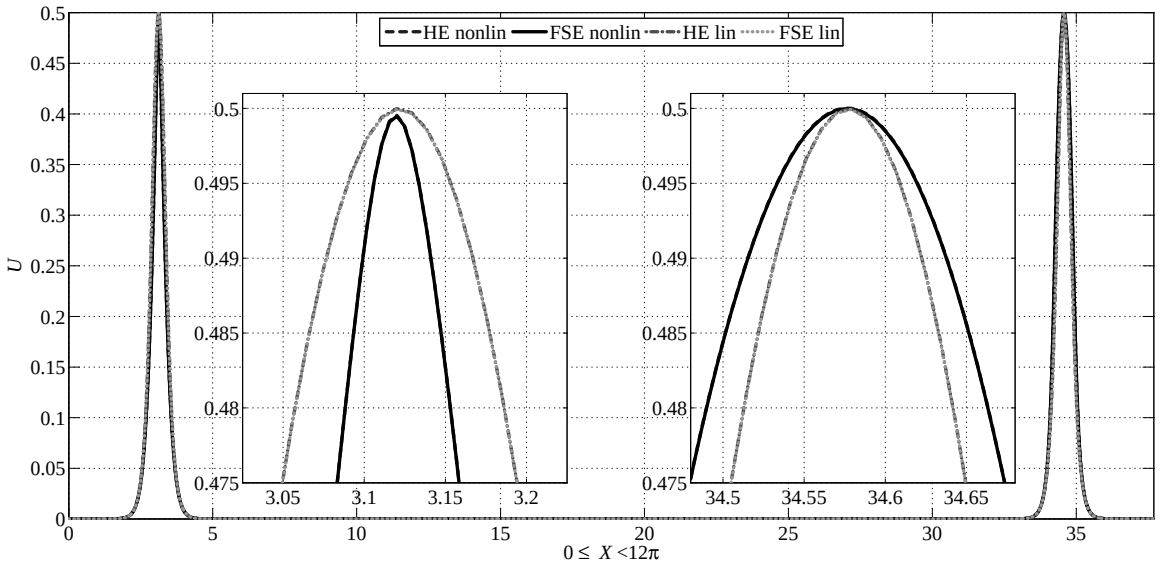

Fig. 2. Waveprofiles at the end of the integration interval for $\gamma_A^2 = 0.05$ and $\gamma_1^2 = 0.9$ (point P1 in Fig. 1).

in linear as well as in nonlinear cases. In order to measure the difference between solutions of the HE and FSE, we introduce the quantity

$$\Delta^S = \sum_{i=1}^{n} \frac{\Delta_i}{n}, \quad \text{where} \quad \Delta_i = \left| U^{\mathrm{HE}}(X_i, T_f) - U^{\mathrm{FSE}}(X_i, T_f) \right|, \tag{10}$$

and n is the number of gridpoints. In the linear case $\Delta^S = 4.98 \times 10^{-6}$ and in the nonlinear case $\Delta^S = 5.15 \times 10^{-6}$ at point P1.

At point P9 the agreement between the solutions of the HE and FSE is good. In Fig. 3 waveprofiles are plotted at the end of the integration interval (when three interactions between the emerged solitary waves have taken place). All waveprofiles are asymmetric. Like at point P1 the left pulse in Fig. 3 is propagating to the right and the right pulse is propagating to the left. One can see that in the nonlinear case again the right

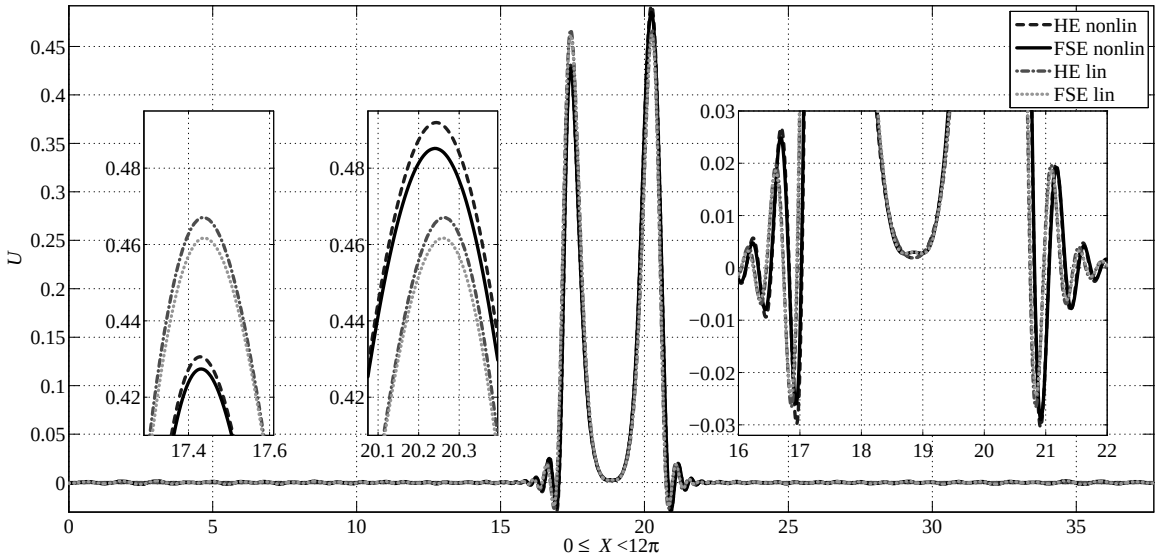

Fig. 3. Waveprofiles at the end of integration for $\gamma_A^2 = 0.45$ and $\gamma_1^2 = 0.5$ (point P9 in Fig. 1).

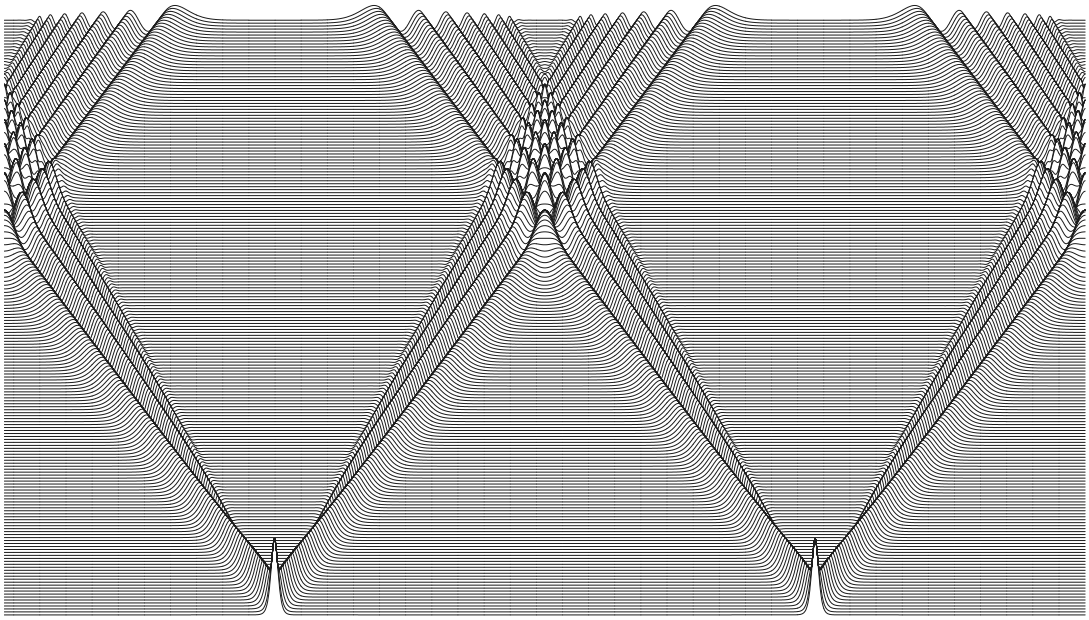

Fig. 4. Time-slice plot of the solution of the linear HE for $\gamma_A^2 = 0.9$ and $\gamma_1^2 = 0.05$ (point P18 in Fig. 1).

propagating wave is sharper and lower than the left propagating wave. However, now waves that correspond to the FSE are visibly lower than these of the HE. In the linear case both the right and left propagating waves have the same amplitude, and symmetry $U(x-6\pi,t) = U(6\pi - x,t)$. In all cases a small tail is formed behind the solitary wave. In nonlinear cases the tails have higher amplitudes than in the linear case. In the linear case $\Delta^S = 8.02 \times 10^{-4}$ and in the nonlinear case $\Delta^S = 8.17 \times 10^{-4}$ at P9.

In order to characterize the time-space behaviour of the solution at point P18, the time-slice plot over two space periods is presented in Fig. 4. In the present case the initial solitary wave is deformed to the wave having the shape similar to the Airy function $\mathrm{Ai}(X)$. Single waveprofiles in Fig. 5 demonstrate that after one interaction of the two emerging wave structures the agreement between the solutions of the HE and

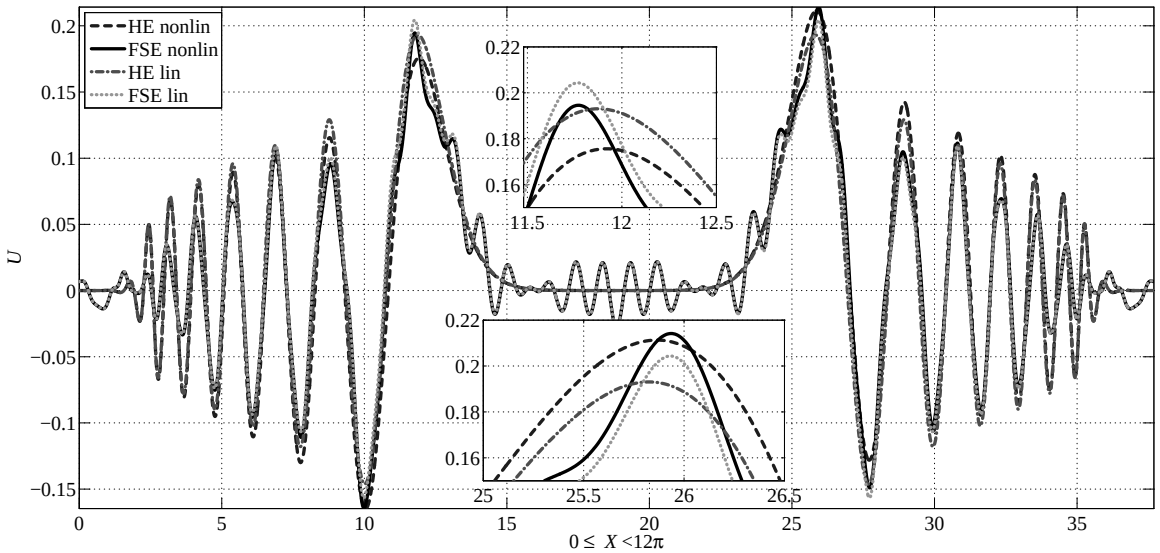

Fig. 5. Waveprofiles at the end of integration for $\gamma_A^2 = 0.9$ and $\gamma_1^2 = 0.05$ (point P18 in Fig. 1).

FSE is good at P18. Like at points P1 and P9 the waves propagating to the left and to the right have equal amplitudes in linear cases. However, now the amplitude is higher in case of the FSE. In the nonlinear case the situation is similar to that of at points P1 and P9 – waves that propagate to the right are lower than those propagating to the left. Unlike in previous cases, additional oscillations that propagate in front of the main wave-structure are generated for the FSE. These oscillations are practically identical in linear and nonlinear cases (see Fig. 5). In the linear case $\Delta^S = 0.0185$ and in the nonlinear case $\Delta^S = 0.0190$ at P18.

4. DISCUSSION AND CONCLUSIONS

Moving along the weak normal dispersion line $\Gamma = 0.05$ (Fig. 1) to the right (γ_A^2 increases), the differences between the solutions of the HE and FSE increase (Fig. 6).

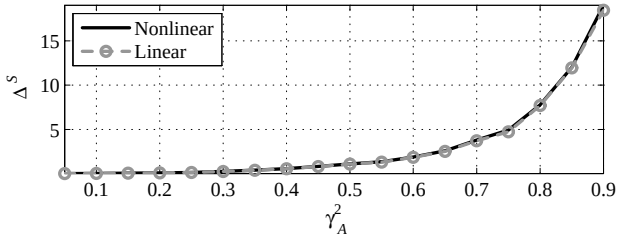

Fig. 6. Quantity Δ^S against γ_A^2 at $T = 100$.

As noted above, there are significant oscillations in front of the propagating wave-structure for higher values of γ_A^2 in case of the FSE (Fig. 5). In case of the HE one cannot detect such oscillations (Figs 4 and 5). This might be due to the fact that according to the dispersion analysis carried out in [18], the FSE has besides the acoustic dispersion curve, a second higher frequency curve. This so-called optical branch reflects internal degrees of freedom according to the hypothesis in [16] and can have a visible effect on the solutions of the FSE, similar to the results shown, for example, in [18]. However, the emergence and origin of those oscillations need futher analysis.

Overall, we may conclude that if we stay in the domain of parameters, where according to the dispersion analysis the difference between dispersion curves of the HE and FSE is less than 5%, we have, indeed, a good agreement between solutions of the HE and FSE. Specifically: (i) predictions from the dispersion analysis hold also for the nonlinear cases, however, the nonlinearity introduces additional effects not taken into account by the linear dispersion analysis; (ii) following the weak normal dispersion line, the agreement between the solutions of the HE and FSE weakens if γ_A^2 increases; (iii) the nonlinearity amplifies the asymmetry between the waveprofiles propagating in opposite directions.

As the interactions between waveprofiles propagating in opposite directions are not entirely elastic, the effect of interactions on the evolution of those waveprofiles needs detailed analysis as done in [28] for the solitary waves that correspond to the HE.

ACKNOWLEDGEMENTS

The authors thank Prof. Jüri Engelbrecht, MSc. Merle Randrüüt, and MSc. Tanel Peets for helpful discussions and comments and Dr Pearu Peterson for Python-related scientific software developments and assistance. The research was supported by the Estonian Science Foundation (grant No. 7035).

REFERENCES

1. Christov, C. I., Maugin, G. A., and Porubov, A. V. On Boussinesq's paradigm in nonlinear wave propagation. *C. R. Mecanique*, 2007, **335**, 521–535.

2. Engelbrecht, J. and Pastrone, F. Waves in microstructured solids with nonlinearities in microscale. *Proc. Estonian Acad. Sci. Phys. Math.*, 2003, **52**, 12–20.
3. Engelbrecht, J., Berezovski, A., Pastrone, F., and Braun, M. Waves in microstructured materials and dispersion. *Phil. Mag.*, 2005, **85**, 4127–4141.
4. Eringen, A. C. *Microcontinuum Field Theories I: Foundations and Solids*. Springer, Berlin, 1999.
5. Erofeev, V. I. *Wave Processes in Solids with Microstructure*. World Scientific, Singapore, 2003.
6. Fornberg, B. *A Practical Guide to Pseudospectral Methods*. Cambridge University Press, Cambridge, 1998.
7. Frigo, M. and Johnson, S. G. The design and implementation of FFTW3. *Proc. IEEE*, 2005, **93**, 216–231.
8. Hindmarsh, A. C. Odepack, a systematized collection of ODE solvers. In *Scientific Computing* (Stepleman, R. S. et al., eds). North-Holland, Amsterdam, 1983, 55–64.
9. Ilison, L. and Salupere, A. Propagation of sech^2-type solitary waves in hierarchical KdV-type systems. *Math. Comput. Simulat.*, 2009, **79**, 3314–3327.
10. Ilison, L., Salupere, A., and Peterson, P. On the propagation of localized perturbations in media with microstructure. *Proc. Estonian Acad. Sci. Phys. Math.*, 2007, **56**, 84–92.
11. Janno, J. and Engelbrecht, J. An inverse solitary wave problem related to microstructured materials. *Inverse Problems*, 2005, **21**, 2019–2034.
12. Janno, J. and Engelbrecht, J. Solitary waves in nonlinear microstructured materials. *J. Phys. A: Math. Gen.*, 2005, **38**, 5159–5172.
13. Jones, E., Oliphant, T., Peterson, P. et al. SciPy: Open source scientific tools for Python, http://www.scipy.org, 2007.
14. Kreiss, H.-O. and Oliger, J. Comparison of accurate methods for the integration of hyperbolic equations. *Tellus*, 1972, **30**, 341–357.
15. Maugin, G. *Nonlinear Waves in Elastic Crystals*. Oxford University Press, Oxford, 1999.
16. Metrikine, A. V. On causality of the gradient elasticity models. *J. Sound Vib.*, 2006, **297**, 727–742.
17. Mindlin, R. D. Micro-structure in linear elasticity. *Arch. Rat. Mech. Anal.*, 1964, **16**, 51–78.
18. Peets, T. and Tamm, K. Dispersion analysis of wave motion in microstructured solids. In *IUTAM Symposium on Recent Advances of Acoustic Waves in Solids* (Tsung-Tsong Wu and Chien-Ching Ma, eds). Springer, Berlin, 2009 (accepted).
19. Peets, T., Randrüüt, M., and Engelbrecht, J. On modelling dispersion in microstructured solids. *Wave Motion*, 2008, **45**, 471–480.
20. Peterson, P. F2PY: Fortran to Python interface generator, http://cens.ioc.ee/projects/f2py2e/ (2005).
21. Porubov, A. V. *Amplification of Nonlinear Strain Waves in Solids*. World Scientific, Hong Kong, 2003.
22. Randrüüt, M. and Braun, M. On one-dimensional solitary waves in microstructured solids. *Wave Motion*, 2010, **47**, 217–230.
23. Randrüüt, M., Salupere, A., and Engelbrecht, J. On modelling wave motion in microstructured solids. *Proc. Estonian Acad. Sci.*, 2009, **58**, 241–246.
24. Salupere, A. The pseudospectral method and discrete spectral analysis. In *Applied Wave Mathematics* (Quak E. and Soomere, T., eds). Springer, Berlin, 2009, 301–334.
25. Salupere, A., Engelbrecht, J., and Peterson, P. On the long-time behaviour of soliton ensembles. *Math. Comput. Simulat.*, 2003, **62**, 137–147.
26. Salupere, A., Tamm, K., Engelbrecht, J., and Peterson, P. On the interaction of deformation waves in microstructured solids. *Proc. Estonian Acad. Sci. Phys. Math.*, 2007, **56**, 93–99.
27. Salupere, A., Ilison, L., and Tamm, K. On numerical simulation of propagation of solitons in microstructured media. In *Proceedings of the 34th Conference on Applications of Mathematics in Engineering and Economics (AMEE '08), Volume 1067 of AIP Conference Proceedings* (Todorov, M. D., ed.). American Institute of Physics, 2008, 155–165.
28. Salupere, A., Tamm, K., and Engelbrecht, J. Numerical simulation of interaction of solitary deformation waves in microstructured solids. *Int. J. Non-Linear Mech.*, 2008, **43**, 201–208.

Üksiklainete formeerumine Mindlini-tüüpi mikrostruktuursetes tahkistes

Kert Tamm ja Andrus Salupere

Lainelevi modelleerimiseks Mindlini-tüüpi mikrostruktuursetes tahkistes on kasutatud Jüri Engelbrechti ja Franco Pastrone tuletatud mudelit. Vaadeldav mudel kirjeldab mikrostruktuuriga füüsikaliselt mittelineaarset materjali, kus mittelineaarsus esineb nii mikro- kui makrotasandil. Numbrilised lahendid on leitud nn täielikule võrrandisüsteemile (4) ja sellest allutusprintsiibi abil tuletatud hierarhilisele võrrandile (5). Saadud lahendeid on võrreldud nii lineaarsel kui mittelineaarsel juhul. On näidatud, et vaadeldud parameetrite piirkonnas on lahendite kokkulangevus hea.